Polyhedron 28 (2009) 2377–2384

Contents lists available at ScienceDirect

Polyhedron

journal homepage: www.elsevier.com/locate/poly

Novel rhenium(III) complexes with the picolinate ligand: Synthesis, spectroscopic investigations, X-ray structures and DFT calculations for $[ReX_2(pic)(PPh_3)_2]$ complexes

B. Machura [a,*], M. Wolff [a], R. Kruszynski [b], J. Mroziński [c], J. Kusz [d]

[a] Department of Crystallography, Institute of Chemistry, University of Silesia, 9th Szkolna St., 40-006 Katowice, Poland
[b] Department of X-ray Crystallography and Crystal Chemistry, Institute of General and Ecological Chemistry, Lodz University of Technology,116 Żeromski St., 90-924 Łódź, Poland
[c] Faculty of Chemistry, Wroclaw University, F. Joliot-Curie 14 St., 50-383 Wrocław, Poland
[d] Institute of Physics, University of Silesia, 4th Uniwersytecka St., 40-006 Katowice, Poland

ARTICLE INFO

Article history:
Received 24 March 2009
Accepted 1 May 2009
Available online 23 May 2009

Keywords:
Keywords
Rhenium complexes
Picolinate ligand
X-ray
Electronic structure
DFT calculations, magnetic measurement

ABSTRACT

The paper presents a combined experimental and computational study of novel rhenium(III) complexes with the picolinate ligand – $[ReCl_2(pic)(PPh_3)_2]$ (**1**) and $[ReBr_2(pic)(PPh_3)_2]$ (**2**). Both complexes **1** and **2** have been characterised spectroscopically and structurally (by single-crystal X-ray diffraction). Complex **1** has been additionally studied by magnetic measurement. The magnetic behavior is characteristic of a mononuclear d^4 low-spin octahedral Re(III) complex ($^3T_{1g}$ ground state) and arises because of the large spin–orbit coupling ($\zeta = 2500\ cm^{-1}$), which gives a diamagnetic ground state. DFT and time-dependent (TD)DFT calculations have been carried out for complex **1**, and UV–vis spectra of the $[ReX_2(pic)(PPh_3)_2]$ compounds have been discussed on this basis.

1. Introduction

The coordination chemistry of rhenium is a field of current growing interest from various viewpoints. The attention of scientists concentrates on synthetic aspects, structural, physicochemical properties and reactivity, as well as on topics with an applied character such as the development of radiotherapeutic cancer agents, nitrogen fixation and catalysis [1]. The ^{186}Re (1.07 MeV β-emitter, $t_{1/2}$ 90 h) and ^{188}Re (2.12 MeV β-emitter, $t_{1/2}$ 17 h) isotopes are among the most attractive isotopes for applications in targeted radionuclide therapy [2,3].

Diazenido and dinitrogen rhenium complexes are important in view of their significance in the field of nitrogen fixation [4–6]. Methyltrioxorhenium is one of the most versatile catalysts for olefin oxidation reactions, aldehyde olefination and olefin metathesis [7,8]. The *mer, trans*-$[ReOCl_3(PPh_3)_2]$ and its derivatives catalyze the oxidation of sulfides to sulfoxides, thiols to disulfides and catalyze oxygen-transfer from sulfoxides to phosphines [8]. The $[ReOCl_2(O–N)(PPh_3)]$ chelates with pyridinecarboxylate ligands exhibit a remarkable catalytic activity for the conversion of ethane to a mixture of propionic and acetic acids in a single-pot process [9]. The $[CH_3ReO(pic)_2]$ complex is an active precursor in olefin oxidation and forms epoxides in a two-phase H_2O_2–H_2O/CH_2Cl_2 system [10].

Generally, chelation of nitrogenous π-acidic ligands to Re^VO facilitates the oxygen atom transfer to oxophilic substrates *via* electron withdrawal from the metal [11]. In this context, the design, synthesis and reactivity of oxorhenium complexes has become the aim of several laboratories, including ours.

Previously, we investigated the reactivity of $[ReOX_3(EPh_3)_2]$ (X = Cl, Br; E = P or As) oxorhenium(V) species towards 1,10-phenanthroline and 5,6-diphenyl-3-(2-pyridyl)-1,2,4-trazine. The products of these reactions include both Re(V) oxocomplexes – $[ReOCl_3(phen)]$ and Re(III) compounds – $[ReCl_2(phen)(PPh_3)_2](ReO_4)\cdot\frac{1}{2}H_2O$, $[ReCl_3(OPPh_3)(dppt)]$ [12,13]. In this report we focus on the examination of the reactions of $[ReOX_3(PPh_3)_2]$ with 1-(2-pyridylcarbonyl)benzotriazole. Potentially, 1-(2-pyridylcarbonyl)benzotriazole can bind to the metal center ion *via* one of two modes: either through the two nitrogen atoms located in the pyridine and triazole rings or through one pyridyl nitrogen and the carbonyl oxygen (Scheme 1).

The reactions of $[ReOX_3(PPh_3)_2]$ with 1-(2-pyridylcarbonyl)benzotriazole lead to novel Re(III) $[ReX_2(pic)(PPh_3)_2]$ complexes (Scheme 2).

The 1-(2-pyridylcarbonyl)benzotriazole hydrolyzes in the reaction with $[ReOX_3(PPh_3)_2]$, and the formed picolinic acid coordinates to the rhenium ion. With much higher yield, however,

* Corresponding author.
E-mail addresses: basia@ich.us.edu.pl (B. Machura), rafal.kruszynski@p.lodz.pl (R. Kruszynski), jmroz@wchuwr.chem.uni.wroc.pl (J. Mroziński).

0277-5387/$ - see front matter © 2009 Elsevier Ltd. All rights reserved.
doi:10.1016/j.poly.2009.05.032

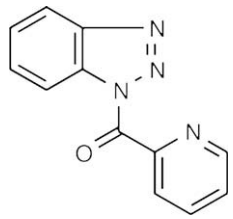

Scheme 1. Structure of 1-(2-pyridylcarbonyl)benzotriazole.

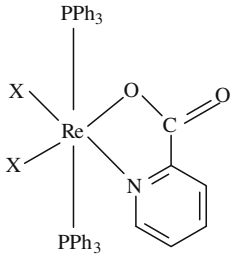

Scheme 2. Structure of $[ReCl_2(pic)(PPh_3)_2]$; X = Cl for **1** and X = Br for **2**.

$[ReCl_2(pic)(PPh_3)_2]$ (**1**) and $[ReBr_2(pic)(PPh_3)_2]$ (**2**) were isolated from the reactions of $[ReOX_3(PPh_3)_2]$ with picolinic acid in the presence of PPh_3 in ethanol.

The molecular orbital diagram of **1** has been calculated with the density functional theory (DFT) method. Currently the density functional theory (DFT) is commonly used to examine the electronic structure of transition metal complexes. It meets with the requirements of being accurate, easy to use and fast enough to allow the study of relatively large molecules of transition metal complexes [14]. The electronic spectrum of **1** has been discussed on the basis of the time-dependent DFT calculations. Recent studies have supported the TDDFT method to be applicable for open- and closed-shell 5d-metal complexes (including rhenium complexes), giving good assignments of the experimental spectra [15–17].

2. Experimental

2.1. General procedure

The reagents used in the syntheses were commercially available and were used without further purification. The $[ReOX_3(PPh_3)_2]$ complexes were prepared according to the literature methods [18]. IR spectra were recorded on a Nicolet Magna 560 spectrophotometer in the spectral range 4000–400 cm^{-1} with the samples in the form of KBr pellets. Electronic spectra were measured on a spectrophotometer Lab Alliance UV–vis 8500 in the range 1000–180 nm in acetonitrile solution. Elemental analyses (C, H, N) were performed on a Perkin–Elmer CHN-2400 analyzer. The ^1H NMR spectrum was obtained in d_6-DMSO using a Bruker Avance 400 spectrometer.

2.2. Preparation of $[ReCl_2(pic)(PPh_3)_2]$ (**1**)

2.2.1. Method A

$[ReOCl_3(PPh_3)_2]$ (0.50 g, 0.6 mmol) was added to 1-(2-pyridylcarbonyl)benzotriazole (0.135 g, 0.6 mmol) in ethanol (100 ml) and the reaction mixture was refluxed for 4 h. The resulting reaction mixture was reduced in volume to ~10 ml and allowed to cool to room temperature. An orange crystalline precipitate of **1** was filtered off and dried in air. Yield 55%.

2.2.2. Method B

$ReOCl_3(PPh_3)_2$] (0.50 g, 0.6 mmol) was added to picolinic acid (0.075 g, 0.61 mmol) and PPh_3 (0.30 g, 1.15 mmol) in ethanol (100 ml) and the reaction mixture was refluxed for 4 h. The resulting reaction mixture was reduced in volume to ~10 ml and allowed to cool to room temperature. An orange crystalline precipitate of **1** was filtered off and dried in air. Yield 80%.

IR (KBr; ν/cm^{-1}): 1697 (vs) ν_{asymCO_2}; 1616 (m) and 1596 (w) ν_{CN} and $\nu_{C=C}$; 1288(s) ν_{asymCO_2}.

Anal. Calc. for $C_{42}H_{34}Cl_2NO_2P_2Re$: C, 55.82; H, 3.79; N, 1.55%. Found: C, 55.61; H, 3.56; N, 1.72%.

2.3. Preparation of $[ReBr_2(pic)(PPh_3)_2]$ (**2**)

A procedure similar to that for $[ReCl_2(pic)(PPh_3)_2]$ was used with $[ReOBr_3(PPh_3)_2]$ (0.50 g, 0.52 mmol) and 1-(2-pyridylcarbonyl)benzotriazole (0.12 g, 0.53 mmol) in method A, and $[ReOBr_3(PPh_3)_2]$ (0.50 g, 0.52 mmol), picolinic acid (0.068 g, 0.55 mmol) and PPh_3 (0.29 g, 1.10 mmol) in method B.

IR (KBr; ν/cm^{-1}): 1684 (vs) ν_{asymCO_2}; 1608 (m) and 1586 (w) ν_{CN} and $\nu_{C=C}$; 1281(s) ν_{asymCO_2}.

Anal. Calc. for $C_{42}H_{34}Br_2NO_2P_2Re$: C, 50.82; H, 3.45; N, 1.41%. Found: C, 50.59; H, 3.32; N, 1.34%.

2.4. Crystal structure determination and refinement

The X-ray intensity data of **1** and **2** were collected on a KM-4-CCD automatic diffractometer equipped with a CCD detector and graphite monochromated Mo Kα radiation (λ = 0.71073 Å) at room temperature. Details concerning crystal data and refinement are given in Table 1. Lorentz, polarization and absorption corrections [19] were applied. The structures were solved by the Patterson method and subsequently completed by difference Fourier recycling. All the non-hydrogen atoms were refined anisotropically using the full-matrix, least-squares technique. The hydrogen atoms were treated as "riding" on their parent carbon atoms and assigned isotropic temperature factors equal to 1.2 times the value of equivalent temperature factor of the parent atom. SHELXS97 [20], SHELXL97 [21] and SHELXTL [22] programs were used for all the calculations. Atomic scattering factors were those incorporated in the computer programs.

2.5. Computational details

The gas phase geometry of **1** was optimized without any symmetry restrictions in the singlet and triplet ground-states with the DFT method using the hybrid B3LYP functional of GAUSSIAN-03 [23–25]. The calculations were performed using the ECP basis set LANL2DZ [26] with an additional *d* and *f* function with the exponent α = 0.3811 and α = 2.033 [27] for rhenium and the standard 6-31G basis set for the other atoms. For chloride, oxygen, nitrogen and phosphorous atoms, diffuse and polarization functions were added [28–33]. The vibrations in the calculated vibrational spectrum of **1** were real, thus the geometry corresponds to a true energy minimum.

The electronic spectrum of **1** was calculated with the TDDFT method, and the solvent effect (acetonitrile) was simulated using the polarizable continuum model with the integral equation formalism (IEF-PCM) [34–37].

2.6. Magnetic measurement

Magnetic measurements of **1** in the temperature range 1.8–300 K were performed using a Quantum Design SQUID-based MPMSXL-5-tpe magnetometer. The superconducting magnet was generally operated at a field strength ranging from 0 to 5 T.

Table 1
Crystal data and structure refinement for complexes **1** and **2**.

	1	**2**
Empirical formula	$C_{42}H_{34}Cl_2NO_2P_2Re$	$C_{42}H_{34}Br_2NO_2P_2Re$
Formula weight	903.74	992.66
Temperature (K)	293.0(2)	100(2)
Wavelength (Å)	0.71073	0.71073
Crystal system	orthorhombic	orthorhombic
Space group	Abm2	Abm2
Unit cell dimensions		
a (Å)	9.3610(2)	9.3877(2)
b (Å)	25.0585(10)	24.7704(8)
c (Å)	15.8943(6)	15.8178(3)
Volume, Å^3	3728.4(2)	3678.23(17)
Z	4	4
Density (calculated) (Mg/m^3)	1.610	1.793
Absorption coefficient (mm^{-1})	3.526	5.601[1]
F(000)	1792	1936
Crystal size, mm	0.004 × 0.006 × 0.093	0.052 × 0.056 × 0.34
θ Range for data collection (°)	1.63–25.04	3.06–25.03
Index ranges	$-11 \leqslant h \leqslant 11$ $-29 \leqslant k \leqslant 29$ $-15 \leqslant l \leqslant 18$	$-11 \leqslant h \leqslant 11$ $-29 \leqslant k \leqslant 29$ $-18 \leqslant l \leqslant 11$
Reflections collected	18 291	12 642
Independent reflections	3131 (R_{int} = 0.0583)	2347 (R_{int} = 0.0243)
Completeness to 2θ (%)	100	99.7
Max. and min. transmission	0.990 and 0.971	0.751 and 0.688
Data/restraints/parameters	3131/1*/244	2347/1*/244
Absolute structure parameter	−0.022(9)	0.002(6)
Goodness-of-fit on F^2	1.088	1.042
Final *R* indices [$I > 2(I)$]	R1 = 0.0292 wR2 = 0.0609	R1 = 0.0147 wR2 = 0.0349
R indices (all data)	R1 = 0.0379 wR2 = 0.0777	R1 = 0.0152 wR2 = 0.0349
Largest difference in peak and hole (e Å^{-3})	1.288 and −0.869	0.632 and −0.452

[*] Restraint of floating origin.

Measurements were made at a magnetic field of 0.5 T. Corrections are based on subtracting the sample-holder signal and the contribution χ_D estimated from Pascal constants equals -499×10^{-6} cm^{3}mol^{-1} for complex **1**. The effective magnetic moment was calculated from the equation, $\mu_{eff} = 2.83(\chi_M T)^{1/2}$ (*B.M.*).

3. Results and discussion

The $[ReCl_2(pic)(PPh_3)_2]$ (**1**) and $[ReBr_2(pic)(PPh_3)_2]$ (**2**) complexes were first isolated from the reactions of $[ReOX_3(PPh_3)_2]$ (X = Cl or Br) with 1-(2-pyridylcarbonyl)benzotriazole in ethanol. Although mechanism of the reaction has not been examined in detail, two reaction courses can be supposed.

The first one is thought to occur *via* reduction of $[ReOX_3(PPh_3)_2]$ by triphenylphosphine and coordination of 1-(2-pyridylcarbonyl)benzotriazole to the Re(III) center. After the coordination of 1-(2-pyridylcarbonyl)benzotriazole to the Re(III) ion, hydrolysis of 1-(2-pyridylcarbonyl)benzotriazole occurs and the picolinic acid formed coordinates to the Re(III) ion to give $[ReCl_2(pic)(PPh_3)_2]$, whereas the benzotriazole remains uncoordinated. The oxygen atom transfer is believed to proceed *via* initial nucleophilic attack on the Re≡O π^* orbitals, and many instances of formation of phosphine oxides from Re^VO and tertiary phosphines can be given [11,38,39]. The starting oxo complex is synthesised using a large excess of triphenylphosphine and it can be impure with PPh_3. The $[ReCl_3(L\text{-}L)(PPh_3)]$ complex with coordinated 1-(2-pyridylcarbonyl)benzotriazole (L-L) has not been isolated from the reaction, but many instances of the formation of $[ReCl_3(L\text{-}L)(PPh_3)]$ in related syntheses can be given [11,38,39].

The second probable reaction model involves hydrolysis of 1-(2-pyridylcarbonyl)benzotriazole, coordination of the picolinate ligand to Re(V), formation of $[ReOCl_2(pic)(PPh_3)_2]$ and subsequent reduction of $[ReOCl_2(pic)(PPh_3)_2]$ to $[ReCl_3(pic)(PPh_3)_2]$. The low yield of $[ReX_2(pic)(PPh_3)_2]$ in the reactions of $[ReOX_3(PPh_3)_2]$ with 1-(2-pyridylcarbonyl)benzotriazole results from an insufficient amount of PPh_3.

With a much higher yield, compounds **1** and **2** were isolated from the reactions of $[ReOX_3(PPh_3)_2]$ with picolinic acid in the presence of PPh_3. In this case, similar reaction models can be postulated. The more probable one seems to involve coordination of the picolinate ligand to Re(V), formation of $[ReOCl_2(pic)(PPh_3)_2]$ and subsequent reduction of $[ReOCl_2(pic)(PPh_3)_2]$ to $[ReCl_3(pic)(PPh_3)_2]$. It has been previously proven that $[ReOCl_3(PPh_3)_2]$ easily reacts with picolinic acid to give $[ReOCl_2(pic)(PPh_3)]$ [9]. However, the other reaction course involving reduction of Re(V) to Re(III) followed by coordination of picolinate ion to the Re(III) is also possible.

The IR spectra of **1** and **2** show features comparable to those of mononuclear picolinato species [40]. The bands assigned to $\nu_{sym}(CO_2)$ and $\nu_{as}(CO_2)$ appear at 1697 and 1288 cm^{-1} for **1**, and 1984 and 1281 cm^{-1} for **2**. The value of $\Delta\nu(CO_2) = \nu_{as}(CO_2) - \nu_s(CO_2)$, equal to ≈400 cm^{-1} for the $[ReX_2(pic)(PPh_3)_2]$ compounds, confirms a unidentate coordination mode of the carboxylate group. Characteristic bands corresponding to the ν(CN) and ν(C=C) modes of the *pic* ligand appear in the range 1620–1550 cm^{-1} [41]. The absence of the strong ν(Re=O) band at ~980 cm^{-1} is a clear indication that there is no oxo-Re(V) starting material left in the samples of **1** and **2**.

The proton spectrum of **1** shows features comparable to those of mononuclear Re(III) with tertiary phosphines. The ^{1}H NMR signals of **1** are relatively narrow due to short electron-spin relaxation time of the Re(III) center, but the signals are spread over the ppm range [42]. The *ortho* protons of two PPh_3 coordinated molecules appear as a doublet at 12.02 ppm, and they are downfield from the *meta* and *para* protons (8.5–8.7 ppm). The three protons of the picolinate ion appear as a triplet at 10.15 ppm and two doublets at 7.13 and 6.81 ppm, respectively.

3.1. Crystal structures

A definite proof for the structure is provided by the X-ray diffraction results. The crystallographic data of the complexes **1** and **2** are summarized in Table 1. The $[ReX_2(pic)(PPh_3)_2]$ complexes are isostructural, crystallise in the orthorhombic Abm2 space group (No. 39) with rhenium, halogen and all the picolinate anion atoms located on the special position *c* with site symmetry m. Thus both the polyhedron $ReCl_2NO$ base and picolinate anion are planar by symmetry.

The short intra- and intermolecular contacts, which can be classified as weak hydrogen bonds [43,44], are gathered in Table 2. The

Table 2
Hydrogen bonds for **1** and **2**.

D–H···A	D–H	H···A	D···A	D–H···A
1				
C(2)–H(2)···Cl(1)	0.93	2.66	3.479(8)	147.9
C(18)–H(18)···O(1)	0.93	2.36	3.105(10)	136.9
C(23)–H(23)···Cl(2)	0.93	2.80	3.378(11)	121.7
2				
C(2)–H(2)···Br(1)	0.93	2.71	3.548(4)	149.8
C(18)–H(18)···O(1)	0.93	2.31	3.068(4)	138.9
C(23)–H(23)···Br(2)	0.93	2.83	3.450(6)	125.2
C(20)–H(20)···Br(2)#1	0.93	2.83	3.615(6)	142.4
C(22)–H(22)···O(2)#2	0.93	2.54	3.320(7)	141.5
C(23)–H(23)···Br(1)#3	0.93	2.77	3.488(6)	135.1

Symmetry transformations used to generate equivalent atoms: #1 −1 + *x*, *y*, *z*; #2 −*x*, *y*, 1/2 + *z*; #3 1−*x*, *y*, 1/2 + *z*.

hydrogen bonding scheme in the both structures is similar due to the isostructurality, however, in **2** some more short contacts exist due to the larger radius of the Br atom. The planar, in the range of experimental error, phenyl rings of the PPh_3 ligands are inclined at 62.4(3), 71.3(3), 81.5(3)° in **1** and at 61.23(3), 71.98(4), 81.25(3)° in **2**. The O–C═O bonds of the carboxylate groups show significant delocalization in both structures (the C(24)–O(1) distances are 1.264(18) and 1.292(8) Å, and the C(24)–O(2) distances are 1.22(2) and 1.248(9) Å, respectively, in **1** and **2**).

The molecular structure of **1** is presented in Fig. 1, and selected bond distances and angles of **1** and **2** are collected in Tables 3 and 4, respectively. The $[ReX_2(pic)(PPh_3)_2]$ complexes show a distorted octahedral geometry about Re with bidentate N,O donors of the picolinato ligand, two halide ions arranged in *cis* geometry and two PPh_3 molecules in *trans* arrangement.

The bond lengths and angles of **1** and **2** do not differ significantly from the expected values for related mononuclear rhenium complexes [9]. The Re–Cl(1) bond *trans* to N is far longer than the Re–Cl(2) bond *trans* to O, indicating a *structural trans* effect of the pyridine ring.

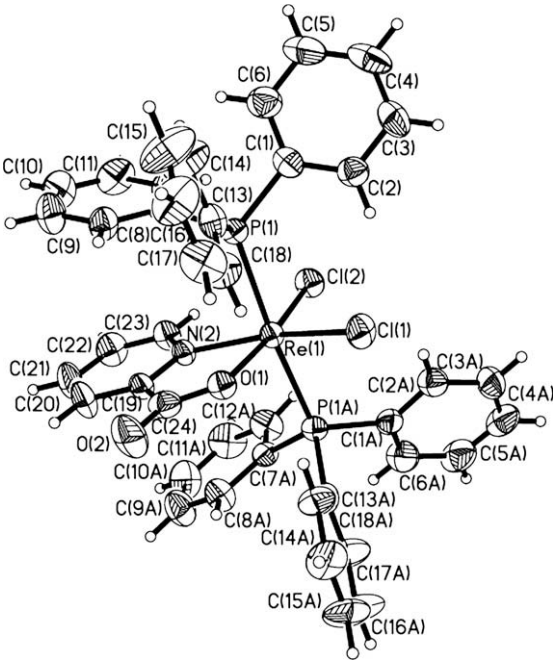

Fig. 1. The molecular structure of **1**.

Table 4
The experimental and optimized bond lengths [Å] and angles [°] for **2**.

Bond lengths	Experimental	Bond angles	Experimental
Re(1)–O(1)	2.044(4)	O(1)–Re(1)–N(2)	76.20(15)
Re(1)–N(2)	2.131(5)	O(1)–Re(1)–Br(2)	170.51(12)
Re(1)–Br(1)	2.5205(6)	N(2)–Re(1)–Br(2)	94.31(14)
Re(1)–Br(2)	2.4906(6)	O(1)–Re(1)–Br(1)	85.44(12)
Re(1)–P(1)	2.4530(8)	N(2)–Re(1)–Br(1)	161.65(14)
		Br(2)–Re(1)–Br(1)	104.04(3)
		O(1)–Re(1)–P(1)	93.99(2)
		N(2)–Re(1)–P(1)	90.93(3)
		Br(2)–Re(1)–P(1)	86.06(3)
		Br(1)–Re(1)–P(1)	90.34(3)
		P(1)–Re(1)–P(1)#1	172.03(5)

3.2. Magnetic properties

The magnetic properties of **1**, in the form μ_{eff} versus T (μ_{eff} is the effective magnetic moment) is shown in Fig. 2. The rhenium(III) complex shows a room temperature magnetic moment of 1.68 B.M. The magnetic moment of the solid is temperature dependent between 300 and 1.8 K and the value of the $\chi_M T$ product decreases on lowering the temperature. This behavior is characteristic of mononuclear d^4 low-spin pseudo-octahedral Re(III) complexes ($^3T_{1g}$ ground state) [45–54] and arises because of the large spin–orbit coupling ($\zeta = 2500\ cm^{-1}$ [55]), which gives a diamagnetic ground state. It seems that at room temperature, in accordance

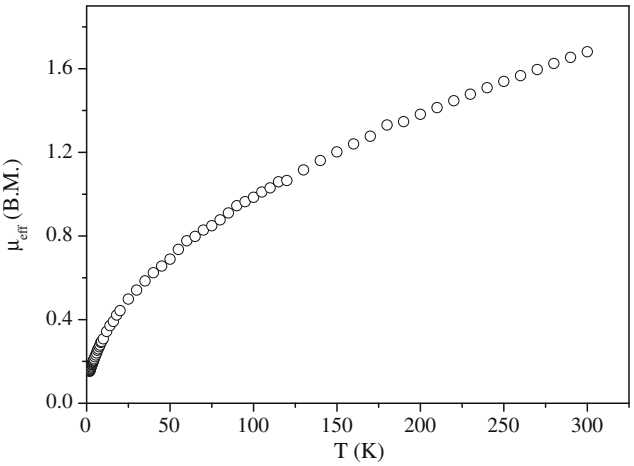

Fig. 2. Plots of experimental effective magnetic moment μ_{eff} (○) vs. temperature for **1**.

Table 3
The experimental and optimized bond lengths [Å] and angles [°] for **1**.

Bond lengths	Experimental	Optimized	Bond angles	Experimental	Optimized
Re(1)–O(1)	2.039(9)	1.941	O(1)–Re(1)–N(2)	75.6(3)	76.20
Re(1)–N(2)	2.143(10)	2.082	O(1)–Re(1)–Cl(2)	169.7(3)	168.47
Re(1)–Cl(1)	2.395(3)	2.503	N(2)–Re(1)–Cl(2)	94.1(3)	92.27
Re(1)–Cl(2)	2.347(3)	2.442	O(1)–Re(1)–Cl(1)	87.6(3)	95.51
Re(1)–P(1)	2.4572(16)	2.481	N(2)–Re(1)–Cl(1)	163.3(3)	171.71
			Cl(2)–Re(1)–Cl(1)	102.66(15)	96.02
			O(1)–Re(1)–P(1)	93.15(6)	91.16
			N(2)–Re(1)–P(1)	91.01(7)	94.46
			Cl(2)–Re(1)–P(1)	86.94(7)	89.72
			Cl(1)–Re(1)–P(1)	89.90(9)	85.61
			P(1)–Re(1)–P(1)#1	173.68(10)	171.09
			O(1)–Re(1)–P(1)#1	93.15(6)	91.70
			N(2)–Re(1)–P(1)#1	91.01(8)	94.46
			Cl(2)–Re(1)–P(1)#1	86.94(7)	89.72
			Cl(1)–Re(1)–P(1)#1	89.90(9)	85.61

Table 5
The energy and character of the selected molecular orbitals with α and β spins for **1**.

	MOs with α spin		MOs with β spin	
	E (eV)	Character	*E* (eV)	Character
HOMO−5	−6.818	$\pi(PPh_3)$	−6.849	$\pi(PPh_3)$, π(Cl)
HOMO−4	−6.779	$\pi(PPh_3)$	−6.820	$\pi(PPh_3)$
HOMO−3	−6.396	π(Cl), n(P) $\pi(PPh_3)$, d_{xz}(Re)	−6.809	$\pi(PPh_3)$
HOMO−2	−6.139	d_{xz}(Re), π(Cl), π(pic)	−6.776	$\pi(PPh_3)$
HOMO−1	−5.821	d_{xy}(Re), π(Cl), π(pic)	−6.342	π(Cl), n(P) $\pi(PPh_3)$
HOMO	−5.818	d_{yz}(Re), π(Cl), π(pic)	−5.298	d_{yz}(Re), π(Cl), π(pic)
LUMO	−2.048	π^*(pic)	−3.148	π^*(Re–Cl), π^*(pic)
LUMO +1	−1.246	π^*(pic)	−2.482	π^*(Re–Cl), π^*(pic)
LUMO+2	−1.028	d^2_z, $\pi^*(PPh_3)$	−1.932	π^*(pic), d_{yz}
LUMO+3	−0.969	$\pi^*(PPh_3)$, d^2_z	−1.239	π^*(pic)
LUMO+4	−0.900	$\pi^*(PPh_3)$	−0.995	$\pi^*(PPh_3)$
LUMO+5	−0.811	$\pi^*(PPh_3)$	−0.891	$\pi^*(PPh_3)$

with Boltzmann's distribution, the higher magnetic state is populated, and it is depopulated with temperature lowering, and a decrease of the magnetic moment is observed.

The magnetization indicates a value of only 0.001 B.M. at 5 T. The magnetization of the sample confirms that the ground state is diamagnetic and the rhenium(III) compound is of a very high purity.

3.3. Geometry optimisation

The gas phase geometry of **1** was optimized in the triplet and singlet states using the DFT method with the B3LYP functional. The total energy of the triplet state is 5.8 kcal/mol smaller in comparison with the singlet state. The optimized geometric parameters of the triplet state are gathered in Table 3. Generally, the predicted bond lengths and angles are in agreement with the values based upon the X-ray crystal structure data, and the general trends observed in the experimental data are well reproduced in the calculations. The largest differences are found for the Re–Cl bond distances. This may come from the basis sets which are approximated to a certain extent or may indicate the influence of the crystal packing on the values of the experimental bond lengths. The theoretical calculations do not consider the effects of chemical environment. However, a similar elongation of the rhenium–chlorine bond lengths (up to 0.25 Å) in the B3LYP with different basis sets has been found in other rhenium–chlorine complexes [56].

3.4. Molecular orbitals

The energies and characters of several of the highest occupied and lowest unoccupied molecular orbitals of **1** are presented in Table 5. Among the highest occupied MOs of **1**, the largest numbers constitute π orbitals of the phenyl rings with a contribution from the Cl atoms. The three highest molecular orbitals with α-spin can be represented as a combination of π^*_{Re-Cl} and π_{pic}, with predominant involvement of the former component. The HOMO orbital, with β-spin, has the same character. The LUMO+1 and LUMO+3 β orbitals of **1** are also to a large extent formed by rhenium d_π atomic orbitals (d_{xz}, d_{yz} or d_{xy}). Among the lowest unoccupied MOs of **1**, the most are constituted of π^* orbitals of the *pic* and phenyl rings. The

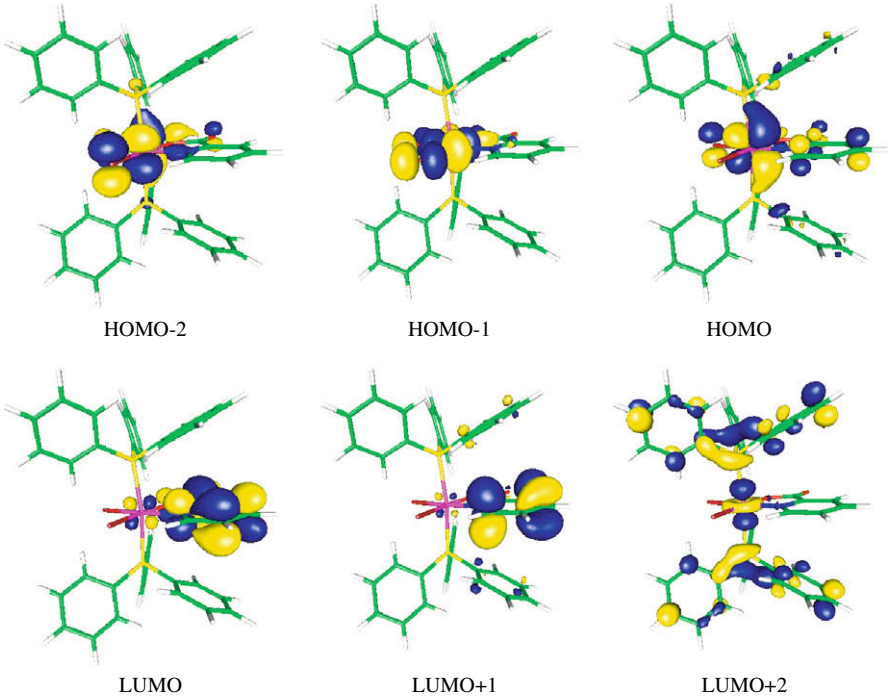

Fig. 3. The selected HOMO and LUMO orbitals with α-spin for **1**.

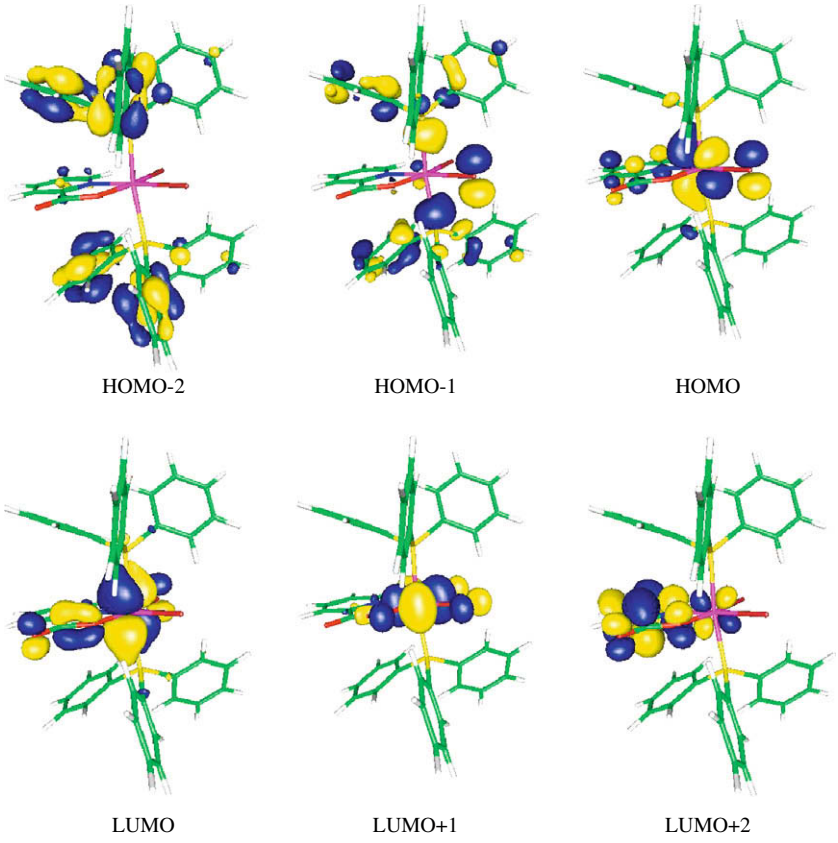

Fig. 4. The selected HOMO and LUMO orbitals with β-spin for **1**.

LUMO and LUMO+1 with α-spin and LUMO+2 and LUMO+3 with β-spin have π^*(pic) character. The π^* phenyl ring orbitals of the triphenylphosphine ligands participate in the higher unoccupied orbitals. The contours of the selected occupied and unoccupied molecular orbitals of **1** with α-spin and β-spin are presented in Figs. 3 and 4, respectively.

3.5. Electronic spectra

The experimental and calculated electronic spectra of **1** are presented in Fig. 5. Each calculated transition is represented by a gaussian function $y = ce^{-bx^2}$ with the height (c) equal to the oscillator strength and b equal to 0.04 nm^{-2}. The electronic spectrum of **2** is very similar in terms of the position, intensity and shape of the bands in the whole region 1000–180 nm; with maxima at 514.1, 458.8, 341.4, 251.5 and 201.7 nm.

Table 6 presents the most important spin-allowed triplet–triplet electronic transitions calculated with the TDDFT method, assigned to the observed absorption bands of **1**. For the high energy part of the spectrum, only transitions with oscillator strengths larger than 0.020 are listed in Table 6. The investigated complex is of a large size; the numbers of basis functions are equal to 832. The calculated electron transitions (1 1 0) do not comprise all the experimental absorption bands; the UV–vis spectrum was calculated to ~270 nm. Thus the shortest wavelength experimental bands of **1** are not assigned to the calculated transitions; some additional intraligand and interligand transitions are expected to be found at higher energies in the calculations for **1**.

The assignment of the calculated orbital excitations to the experimental bands was based on an overview of the contour plots and relative energy to the HOMO and LUMO involved in the electronic transitions.

In the 350–600 nm region, complex **1** displays multiple transitions of moderate intensity in the form of peaks and shoulders.

The low-energy absorption band of **1** originates from the transitions between HOMO-1, HOMO, LUMO and LUMO+2 with β-spin. As can be seen from Fig. 4, the β HOMO−1 is composed of ligand (chloride and triphenylphosphine) orbitals, β HOMO is delocalized on the central ion and ligands, and β LUMO and β LUMO+2 are

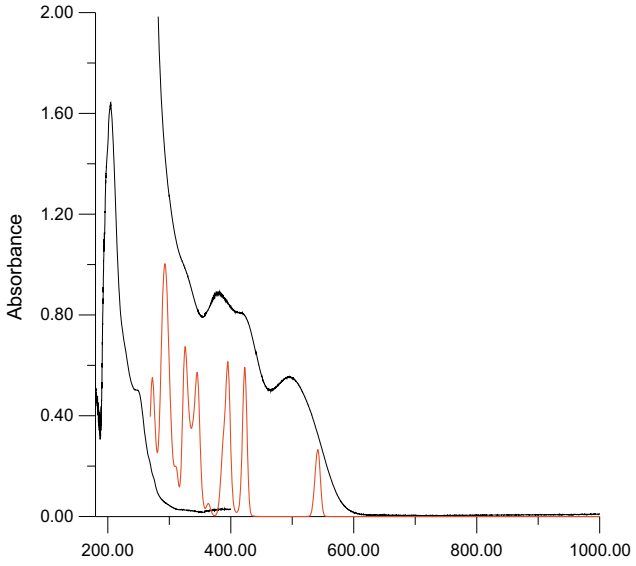

Fig. 5. The experimental (black) and calculated (red) electronic absorption spectra of a solution of **1** in acetonitrile. (For interpretation of the references to colour in this figure legend, the reader is referred to the web version of this article.)

Table 6
The energy and molar absorption coefficients of experimental absorption bands and the electronic transitions calculated with the TDDFT method for **1**.

The most important orbital excitations	Character	Calculated			Experimental Λ (nm) (E [eV]) ε
		λ (nm)	E (eV)	f	
H(β) → L+2(β) H-1(β) → L(β)	d/π(Cl)/π(pic) → π*(pic)/d n(P)/π(PPh_3)/π(Cl) → d/π*(pic)	542.6	2.28	*0.0145*	510.5 (2.43) 3600
H-1(β) → L(β) H(β) → L+2(β)	n(P)π(PPh_3)/π(Cl) → d/π*(pic) d/π(Cl)/π(pic) → π*(pic)/d	537.8	2.31	*0.0067*	
H(α) → L(α)	d/π(Cl)/π(pic) → π*(pic)	422.7	2.93	*0.0389*	427.7 (2.90) 5350
H-2(α) → L(α)	d/π(Cl)/π(pic) → π*(pic)	395.4	3.14	*0.0383*	379.3 (3.27) 6150
H-2(α) → L(α) H(β) → L+3(β)	d/π(Cl)/π(pic) → π*(pic)	388.0	3.20	*0.0162*	
H(α) → L+2(α) H(α) → L+11(α)	d/π(Cl)/π(pic) → d/π*(PPh_3)	345.9	3.58	*0.0296*	328.2 (3.78) 6650
H(β) → L+5(β) H(α) → L+1(α)	d/π(Cl)/π(pic) → π*(PPh_3) d/π(Cl)/π(pic) → π*(pic)	325.2	3.81	*0.0273*	
H-2(α) → L+1(α)	d/π(Cl)/π(pic) → π*(pic)	300.4	4.13	*0.0100*	247.9 (5.00) 87 000
H(α) → L+3(α)	d/π(Cl)/π(pic) → π*(PPh_3)/d	297.0	4.17	*0.0100*	
H(β) → L+9(β) H-5(α) → L(α)	d/π(Cl)/π(pic) → π*(PPh_3) π(PPh_3) → π*(pic)	295.9	4.19	*0.0154*	
H-14(β) → L+1(β)	π(Cl) → d	291.9	4.25	*0.0146*	
H-3(β) → L+2(β)	π(PPh_3) → π*(pic)/d	288.9	4.29	*0.0179*	
					204.8 (6.05) 270 000

ε – Molar absorption coefficient [$dm^3\ mol^{-1}\ cm^{-1}$].
f – Oscillator strength.
H – Highest occupied molecular orbital.
L – Lowest unoccupied molecular orbital.

formed from d_{Re} orbitals and π^*-bonding orbitals of the picolinate ligand. Accordingly, these transitions can be seen as delocalized MLLCT (*Metal–Ligand-to-Ligand CT*) transitions.

The transitions assigned to the experimental bands at 427.7 and 379.3 nm can be seen as mixed Re → π*(pic) (*Metal–Ligand Charge Transfer*; *LMCT*) and π(Cl)/π(pic) → π*(pic) (*Ligand–Ligand Charge Transfer*; *LLCT*) transitions. The experimental absorption band at 328.2 nm is mainly attributed to the d/π(Cl)/π(pic) → d/π*(PPh_3) transition, whereas the transitions assigned to the experimental band at 247.9 are mainly of *LLCT* character.

4. Conclusions

This work is an extension of our previous research on the reactivity of [$ReOX_3(PPh_3)_2$] towards N–O and N–N chelating ligands. 1-(2-Pyridylcarbonyl)benzotriazole does not coordinate to the rhenium ion. Hydrolysis of 1-(2-pyridylcarbonyl)benzotriazole in the reaction with the oxo-complexes occurs and picolinic acid binds to the Re center to give the [$ReX_2(pic)(PPh_3)_2$] complexes (X = Cl, Br). The studied compounds were synthesized for the first time. Their structures were definitively proven by X-ray diffraction measurements and confirmed by spectroscopic analysis. The magnetic measurements, NMR and UV–vis studies confirm that the [$ReX_2(pic)(PPh_3)_2$] complexes are typical mononuclear d^4 low-spin octahedral Re(III) complexes. In the visible region the [$ReX_2(pic)(PPh_3)_2$] complexes display multiple transitions of moderate intensity in the form of peaks and shoulders. The TDDFT/PCM calculations show that these transitions can be seen as delocalized MLLCT (Metal–Ligand-to-Ligand CT) transitions.

Supplementary data

CCDC 724894 and 724895 contain the supplementary crystallographic data for $C_{42}H_{34}Cl_2NO_2P_2Re$ and $C_{42}H_{34}Br_2NO_2P_2Re$. These data can be obtained free of charge via http://www.ccdc.cam.ac.uk/conts/retrieving.html, or from the Cambridge Crystallographic Data Centre, 12 Union Road, Cambridge CB2 1EZ, UK; fax: (+44) 1223-336-033; or e-mail: deposit@ccdc.cam.ac.uk.

Acknowledgements

The GAUSSIAN-03 calculations were carried out in the Wrocław Centre for Networking and Supercomputing, WCSS, Wrocław, Poland, http://www.wcss.wroc.pl, under calculational Grant No. 51/96.

References

[1] U. Abram, in: J.A. McCleverty, T.J. Meyer (Eds.), Comprehensive Coordination Chemistry, second ed., vol. 5, Elsevier, 2003, pp. 271–402 (Chapter 5.3).
[2] J.R. Dilworth, S.J. Parrott, Chem. Soc. Rev. 27 (1998) 43.
[3] P. Blower, J. Chem. Soc., Dalton Trans. (2006) 1705.
[4] R.L. Richards, Coord. Chem. Rev. 154 (1996) 83.
[5] M.D. Fryzuk, S.A. Johnson, Coord. Chem. Rev. 200–202 (2000) 379.
[6] A.J.L. Pombeiro, M.F.C. Guedes da Silva, R.A. Michelin, Coord. Chem. Rev. 218 (2001) 43.
[7] F.E. Kühn, A. Scherbaum, W.A. Herrmann, J. Organomet. Chem. 689 (2004) 4149.
[8] G.S. Owens, J. Arias, M.M. Abu-Omar, Catalysis Today 55 (2000) 317.
[9] A.M. Kirillov, M. Haukka, M.V. Kirillova, A.J.L. Pombeiro, Adv. Synth. Catal. 347 (2005) 1435.
[10] A. Deloffre, S. Halut, L. Salles, J.-M. Brégeault, J.R. Gregorio, B. Denise, H. Rudler, J. Chem. Soc., Dalton Trans. (1999) 2897.
[11] S. Bhattacharyya, I. Chakraborty, B.K. Dirghangi, A. Chakravorty, Chem. Commun. (2000) 1813.
[12] B. Machura, R. Kruszynski, M. Jaworska, J. Kłak, J. Mroziński, Polyhedron 25 (2006) 2537.
[13] B. Machura, R. Kruszynski, J. Kusz, J. Kłak, J. Mroziński, Polyhedron 26 (2007) 4427.
[14] H. Chermette, Coord. Chem. Rev. 178–180 (1998) 699.
[15] M.C. Aragoni, M. Arca, T. Cassano, C. Denotti, F.A. Devillanova, F. Isaia, V. Lippolis, D. Natali, L. Niti, M. Sampietro, R. Tommasi, G. Verani, Inorg. Chem. Commun. 5 (2002) 869.
[16] P. Romaniello, F. Lelj, Chem. Phys. Lett. 372 (2003) 51.
[17] P. Norman, P. Cronstrand, J. Ericsson. Chem. Phys. 285 (2002) 207.
[18] G. Rouschias, G. Wilkinson, J. Chem. Soc. A (1966) 465.
[19] (a) CrysAlis RED, Oxford Diffraction Ltd., Version 1.171.29.2.;
(b) STOE and Cie, X-RED. Version 1.18. STOE & Cie GmbH, Darmstadt, Germany, 1999.
[20] G.M. Sheldrick, Acta Cryst. A46 (1990) 467.
[21] G.M. Sheldrick, SHELXL97. Program for the Refinement of Crystal Structures, University of Gttingen, Germany, 1997.

[22] G.M. Sheldrick, SHELXTL: release 4.1 for Siemens Crystallographic Research Systems, 1990.
[23] Gaussian 03, Revision D.01, M. J. Frisch, G. W. Trucks, H. B. Schlegel, G. E. Scuseria, M. A. Robb, J. R. Cheeseman, J. A. Montgomery, Jr., T. Vreven, K. N. Kudin, J. C. Burant, J. M. Millam, S. S. Iyengar, J. Tomasi, V. Barone, B. Mennucci, M. Cossi, G. Scalmani, N. Rega, G. A. Petersson, H. Nakatsuji, M. Hada, M. Ehara, K. Toyota, R. Fukuda, J. Hasegawa, M. Ishida, T. Nakajima, Y. Honda, O. Kitao, H. Nakai, M. Klene, X. Li, J. E. Knox, H. P. Hratchian, J. B. Cross, V. Bakken, C. Adamo, J. Jaramillo, R. Gomperts, R. E. Stratmann, O. Yazyev, A. J. Austin, R. Cammi, C. Pomelli, J. W. Ochterski, P. Y. Ayala, K. Morokuma, G. A. Voth, P. Salvador, J. J. Dannenberg, V. G. Zakrzewski, S. Dapprich, A. D. Daniels, M. C. Strain, O. Farkas, D. K. Malick, A. D. Rabuck, K. Raghavachari, J. B. Foresman, J. V. Ortiz, Q. Cui, A. G. Baboul, S. Clifford, J. Cioslowski, B. B. Stefanov, G. Liu, A. Liashenko, P. Piskorz, I. Komaromi, R. L. Martin, D. J. Fox, T. Keith, M. A. Al-Laham, C. Y. Peng, A. Nanayakkara, M. Challacombe, P. M. W. Gill, B. Johnson, W. Chen, M. W. Wong, C. Gonzalez, J. A. Pople, Gaussian, Inc., Wallingford CT, 2004.
[24] A.D. Becke, J. Chem. Phys. 98 (1993) 5648.
[25] C. Lee, W. Yang, R.G. Parr, Phys. Rev. B 37 (1988) 785.
[26] P.J. Hay, W.R. Wadt, J. Chem. Phys. 82 (1985) 299.
[27] K. Eichkorn, F. Weigend, O. Treutler, R. Ahlrichs, Theor. Chem. Acc. 97 (1997) 119.
[28] W.J. Hehre, R. Ditchfield, J.A. Pople, J. Chem. Phys. 56 (1972) 2257.
[29] P.C. Hariharan, J.A. Pople, Theoret. Chimica Acta 28 (1973) 213.
[30] M.M. Francl, W.J. Petro, W.J. Hehre, J.S. Binkley, M.S. Gordon, D.J. DeFrees, J.A. Pople, J. Chem. Phys. 77 (1982) 3654.
[31] T. Clark, J. Chandrasekhar, P.v.R. Schleyer, J. Comp. Chem. 4 (1983) 294.
[32] R. Krishnam, J.S. Binkley, R. Seeger, J.A. Pople, J. Chem. Phys. 72 (1980) 650.
[33] P.M.W. Gill, B.G. Johnson, J.A. Pople, M.J. Frisch, Chem. Phys. Lett. 197 (1992) 499.
[34] M.T. Cances, B. Mennucci, J. Tomasi, J. Chem. Phys. 107 (1997) 3032.
[35] M. Cossi, V. Barone, B. Mennucci, J. Tomasi, Chem. Phys. Lett. 286 (1998) 253.
[36] B. Mennucci, J.Tomasi, J. Chem. Phys. 106 (1997) 5151.
[37] M. Cossi, G. Scalmani, N. Rega, V. Barone, J. Chem. Phys. 117 (2002) 43.
[38] I. Chakraborty, S. Bhattacharyya, S. Banerjee, B.K. Dirghangi, A. Chakravorty, J. Chem. Soc., Dalton Trans. (1999) 3747.
[39] S. Sengupta, J. Gangopadhyay, A. Chakravorty, J. Chem Soc., Dalton Trans. (2003) 4635.
[40] A. Deloffre, S. Halut, L. Salles, J.-M. Brégeault, J.R. Gregorio, B. Denise, H. Rudler, J. Chem. Soc., Dalton Trans. (1999) 2897.
[41] K. Nakamoto, Infrared and Raman Spectra of Inorganic and Coordination Compounds, fourth ed., Wiley-Interscience, New York, 1986.
[42] C. Pearson, A.L. Beauchamp, Inorg. Chim. Acta 237 (1995) 13.
[43] G.A. Jeffrey, W. Saenger, Hydrogen Bonding in Biological Structures, Springer-Verlag, 1994.
[44] G.R. Desiraju, T. Steiner, The Weak Hydrogen Bond in Structural Chemistry and Biology, Oxford University Press, 1999.
[45] B. Machura, R. Penczek, R. Kruszyński, J. Kłak, J. Mroziński, J. Kusz, Polyhedron 26 (2007) 4833.
[46] J.E. Fergusson, Coord. Chem. Rev. 1 (1966) 459.
[47] B.N. Figgis, J. Lewis, Prog. Inorg. Chem. 6 (1964) 37.
[48] B.N. Figgis, Introduction to Ligand Field, Wiley-Interscience, New York, 1966. p. 248.
[49] J. Chatt, G.J. Leigh, D.M.P. Mingos, E.W. Randall, D. Shaw, J. Chem. Soc., Chem. Commun. (1968) 419.
[50] H.P. Gunz, G.J. Leigh, J. Chem. Soc. (1971) 2229.
[51] B. Coutinho, J.R. Dilworth, P. Jobanputra, R.M. Thompson, S. Schmidt, J. Strähle, C.M. Archer, J. Chem. Soc., Dalton Trans (1995) 1663.
[52] M. Hirsch-Kuchma, T. Nicholson, A. Davison, W.M. Davis, A.G. Jones, Inorg. Chem. 36 (1997) 3237.
[53] C.A. McConnachie, E.I. Stiefel, Inorg. Chem. 36 (1997) 6144.
[54] C. Pearson, A.L. Beauchamp, Can. J. Chem. 75 (1997) 220.
[55] A. Earnshaw, B.N. Figgis, J. Lewis, R.D. Peacok, J. Chem. Soc. (1961) 3132.
[56] Psaroudakis, K. Mertis, D.G. Liakos, E.D. Simandiras, Chem. Phys. Lett. 369 (2003) 490.